# Integration of tungsten layers for the mass fabrication of WO3-based pH-sensitive potentiometric microsensors

Ahmet Lale, Aliki Tsopela, Aurélie Civélas, Ludovic Salvagnac, Jérôme Launay, Pierre Temple-Boyer

# INTEGRATION OF TUNGSTEN LAYERS FOR THE MASS FABRICATION OF $WO_3$-BASED PH-SENSITIVE POTENTIOMETRIC MICROSENSORS

Ahmet Lale[1,2], Aliki Tsopela[1,2], Aurélie Civélas[1,2], Ludovic Salvagnac[1,2], Jérôme Launay[1,2], Pierre Temple-Boyer[1,2]

[1] CNRS, LAAS, 7 avenue du colonel Roche, F-31400 Toulouse, France

[2] Université de Toulouse, UPS, LAAS, F-31400 Toulouse, France

**Abstract**

($W/WO_3$ –Ag/AgCl) and ($Pt/IrO_2$ – Ag/AgCl) potentiometric microdevices were developed for pH measurement in liquid phase using a (Pt – Pt – Ag/AgCl) electrochemical microcells (ElecCell) silicon-based technological platform. A special emphasis was placed on the mass fabrication of the $W/WO_3$ microelectrode using sputtering deposition and oxygen plasma processes. Compared to the $Pt/IrO_2$-based one, the $W/WO_3$-based microelectrodes showed lower performances regarding the pH measurement. Nevertheless, since $W/WO_3$ microelectrodes yielded quasi-Nernstian sensitivity (around 55 mV/pH) in the [2-12] pH range, tungsten oxide $WO_3$ can be considered as a good candidate for the mass fabrication of pH microsensors using silicon technologies, even if important temporal drift (at least 6 millivolts per hour) and high hysteresis (around 50 mV) were also evidenced.

**Keywords:** microelectrodes, potentiometric microdevices, physical vapour deposition, tungsten W thin films, tungsten oxide $WO_3$, iridium oxide $IrO_2$, pH measurement

## 1. Introduction

Since life-related processes concern mainly water-based samples, pH measurement was required for various analyses and pH monitoring was intensively studied [1]. Optical detection/transduction principles were successfully developed and industrialized for health applications. In order to meet requirements of small volume sample, high screening, high performance and low cost, pH coloured indicators have therefore been used for medical analysis [2]. Regarding environmental applications and food industry, electrochemical detection/transduction principles were preferred. As a result, pH-glass electrodes were widely developed to deal with high sample volumes, long-duration analysis and in-situ process monitoring (even if their use is still hindered by fragility) [3]. Nevertheless, since analysis techniques have followed the miniaturization path, the development of electrochemical detection/transduction principles attracted particular attention due to their higher compatibility with microelectronics, leading to the development of solid-state pH microsensors. On the one hand, pH-sensitive chemical field effect transistors (pH-ChemFET) were studied using different sensitive gate materials such as silicon nitride $Si_3N_4$, aluminium oxide $Al_2O_3$ and tantalum oxide $Ta_2O_5$ [4]. Thus, high compatibility of field effect transistors (FET) microdevices with silicon-based technologies ensured mass fabrication of integrated pH microsensors dedicated to pH measurement [5], bacterial analysis [6], on-line monitoring of cell metabolism [7], on-line biochemical detection [8] as well as genome sequencing [9]. On the other hand, research has been focused on pH-based ion-sensitive electrodes (pH-ISE) and many metal oxides were used as sensitive materials [10].

Among them, iridium oxide $IrO_2$ (or $IrO_x$) was extensively studied. Through the development of anodic electrodeposition processes [11], $IrO_2$ (micro)electrodes were produced, demonstrating near-Nernstian responses, high pH detection range, low interferences of other ionic species and improved long-term stability [12-18]. As a result, these anodically electrodeposited iridium oxide

films (AEIROF) were used for various pH-related applications: pH sensing [14,15,18], pH imaging using scanning electrochemical microscopy [19], biomedical analysis [20], neurostimulation [21], cell media microanalysis [22]. Nevertheless, even if first devices were reported for simultaneous fabrication of AEIROF-based microelectrodes into microfluidic channels [22-24], the integration of $IrO_x$-based pH microsensors is still hindered by low compatibility of anodic electrodeposition with mass fabrication. In order to overcome these limitations, some technological processes were proposed, including thermal oxidation [25], physical vapour deposition [26,27] and sol-gel dip-coating/patterning deposition [28,29]. However, in these different cases, $IrO_x$ (micro)electrodes are still characterized by good pH detection properties but also by non-Nernstian pH responses (sensitivity around 50 mV/pH). Thus, taking into account the mass integration limitation, other metal oxides were studied to compete with iridium oxide $IrO_2$ regarding development of pH microsensors.

In this context, tungsten oxide $WO_3$ (or $WO_x$) is also an interesting candidate and exhibits significant advantages compared to other metal oxides. Firstly, tungsten (W) is a well-known metal in silicon foundries since it has been used to create gate contacts and interconnects in very-large scale integration (VLSI) devices developed for microelectronic applications [30,31]. Secondly, tungsten oxide thin films were studied for the mass fabrication of photo-electrochemical devices while developing integration processes based on physical vapour deposition [32-35]. Thirdly, it was successfully elaborated as a sensitive material for the fabrication of pH-ChemFET microdevices [36] as well as pH-sensitive microelectrodes [37-41]. In most cases, tungsten oxidation was obtained by electro-oxidation in basic solutions, leading to the formation of stable $WO_3$ thin films. Thus, non-Nernstian pH-responses (sensitivity around 55 mV/pH) were evidenced on wide pH range. Lastly, metallic tungsten (W) electrode was investigated as a potential candidate for pH measurement using $WO_2$ or $W_2O_5$ native oxide as pH-sensitive layer, exhibiting lower sensitivity (~ 50 mV/pH) [42]. In most cases, the mass fabrication requirement was not met. Nevertheless, this

last work offers opportunities for the integration of tungsten-based pH-sensitive layers and the development of mass–fabricated $W/WO_3$ pH microsensors using silicon-based technologies.

This paper deals with the integration of pH-sensitive, electrochemical microsensors based on tungsten trioxide. In order to deal with mass fabrication, we have developed a two-step deposition process where we first deposit tungsten (W) via sputtering and then we oxidize the film using an oxygen ($O_2$) plasma to form tungsten trioxide. Thus, $W/WO_3$ integrated microelectrodes are microfabricated using a standard (Pt - Pt – Ag/AgCl) electrochemical microcell (ElecCell) based on silicon technologies. Finally, detection properties of $W/WO_3$ pH-sensitive microelectrodes are studied and compared to standard $Pt/IrO_2$ ones.

## 2. Experimental

### 2.1 Deposition of tungsten thin films

Growth experiments were carried out in a UNIVEX 450C cluster. Magnetron sputter depositions were performed using a tungsten cathode (99.999% purity). Electrical bias and sputtering power were fixed at 0 volt and 800 Watts respectively, while the argon (Ar) total pressure varied between $10^{-3}$ and $3 \times 10^{-2}$ millibar. Thin tungsten films (thickness range: 200 – 500 nm according to experimental conditions) were deposited on 4-inch, around 525 μm thick, (100), oxidized ($SiO_2$ thickness around 600 nm) silicon wafers. Films thickness was measured by profilometry using the shadow mask technique, and deposition rates were calculated by dividing deposited thickness by deposition duration. Then, wafer curvature shifts before and after deposition were also assessed by profilometry. Since the deposited tungsten films are very thin compared to the silicon wafer, its average stress was finally calculated through Stoney's formula [43]. Finally, electrical conductivity of tungsten films was estimated by four-probe measurements. For all these

different characterization techniques, measurement accuracy is estimated between ± 5% and ± 10%. Nevertheless, in order to define more precisely the standard deviations associated to deposition conditions and uniformity, experimental results were deduced from at least five measurements on the wafer.

## 2.2 Electrochemical microcells fabrication

Different pH-sensitive microelectrodes were fabricated using a technological platform dedicated to the microfabrication of electrochemical microcells (ElecCell) [18,44]. Starting with an oxidized (oxide thickness: ~ 0.6 µm) silicon wafer in order to ensure electrical insulation between different metallic layers, two successive evaporation processes were performed using the lift-off technique in order to fabricate (Pt - Pt - Ag) ElecCell microdevices. Firstly, a 120 nm platinum layer was deposited on a 20 nm titanium underlayer in order to enhance platinum adhesion on silicon oxide, followed by a 400 nm silver layer. For tungsten-based microelectrodes, a 500 nm tungsten layer was first deposited on the oxidized substrate without any adhesion layer and patterned using a standard lift-off process in order to enhance fabrication's reproducibility. Tungsten deposition parameters were selected so that technological defects related to residual stress are limited. An oxygen ($O_2$) plasma process was then performed (plasma power: 800 W – duration: 15 min) in order to oxidize the tungsten layer and to form a $WO_3$ thin film on top. Then, typical Ti/Pt and Ag deposition/patterning procedures previously described were used. Finally, an inorganic $Si_3N_4$-based passivation layer (thickness around 0.1 µm) was deposited on the whole wafer. Patterning was performed using an optimized double layer lift-off process in order to define microelectrodes active surface and ensure electrochemical properties in liquid phase [45]. According to the photolithographic masks design, 50µm-diameter disk working microelectrodes were developed (theoretic area: $19.6 \times 10^{-4}$ $mm^2$). In contrast, very large silver-based reference

microelectrodes (~ 0.02 $mm^2$) were fabricated in order to improve the potentiometric detection behaviour.

Thus, ($W/WO_3$ – Pt – Ag) and (Pt – Pt – Ag) microdevices were mass fabricated on silicon substrate. After dicing, ElecCell chips were placed, glued by an epoxy insulating glue and wire bonded on a specifically coated printed circuit. Packaging was completed by encapsulating wire bonds using a silicone glop-top in order to be completely compatible with liquid phase measurement. For the (Pt – Pt – Ag) configuration, an iridium oxide $IrO_2$ thin film was electrodeposited according to methods proposed in literature [11,14,23]. Thus, 0.075 g of iridium tetrachloride $IrCl_4$ was dissolved in 50 mL of deionized water, and the solution was stirred for 30 minutes. Hydrogen peroxide $H_2O_2$ (30%, 0.5 mL) and then 0.25 g of oxalic acid $C_2O_4H_2$ were added in the solution. After a 10-minutes stirring process, solution's pH was adjusted to 10.5 using dehydrated potassium carbonate $K_2CO_3$. Then, the solution was stored for stabilization for one week. Finally, platinum microelectrode was immersed in this iridium-based solution and a potential of 0.6 V was applied using an $Ag/AgCl/KCl_{sat}$ double junction glass electrode as reference. The $IrO_2$ electrodeposition process was finally interrupted when a 0.5 $C/cm^2$ charge was deposited.

Finally, for all microdevices, after an initial Ag surface evaluation by cyclic voltammetry (potential scan rate: 50 mV/s between -1.1 and 0.5 V) in a 0.1 M $KNO_3$-based acid solution (pH = 3.5), the silver/silver chloride Ag/AgCl reference microelectrode was obtained by oxidizing the silver metallic layer in a 0.01 M KCl solution. This oxidation was performed by linear voltammetry (potential scan rate: 1 mV/s between 0 and 0.25 V) using an $Ag/AgCl/KCl_{sat}$ double junction glass electrode as reference. Overall, ($W/WO_3$ – Ag/AgCl) and ($Pt/IrO_2$ – Ag/AgCl) pH-sensitive integrated microdevices were successfully fabricated (figures 1a and 1b).

## 2.3 Electrochemical characterization

All electrochemical characterizations were held using a multi-channel VMP potentiostat from Biologic. In order to define standard deviations associated to microfabrication process and/or characterization procedure, three $Pt/IrO_2$ and six $W/WO_3$ microelectrodes (thanks to the mass fabrication possibility) were characterized. Thus, Nernst potentials were estimated by potentiometry using the open-circuit method. First, electrochemical properties of the integrated Ag/AgCl reference electrode were studied. Using a commercial reference electrode (Metrohm Ag/AgCl glass double junction, with inner and outer compartments filled with KCl 3.5 M), open-circuit potentials at equilibrium were recorded in solutions consisting of a background electrolyte ($CH_3COOLi$ - 0.1 M) with potassium chloride KCl concentrations ranging from $10^{-5}$ M to saturation (~ 4.5 M). Thus, chloride ion ($Cl^-$) detection properties as well as the temporal stability were thoroughly studied. Then, pH measurements were performed for different solutions (pH = 2.0, 4.0, 5.5, 7.0, 8.5, 10.0 and 12.0). Chloride ion's concentration was kept constant for all the buffer samples in order to ensure proper use of the integrated Ag/AgCl reference microelectrode, and compare it to the commercial glass reference electrode. All chemical reagents were purchased from Sigma.

## 3. Results and discussion

### 3.1 Deposition of tungsten thin films

Properties of different sputtered tungsten films were studied as a function of argon total pressure (table 1). Concerning the deposition rate, it is proportional to ions current in the plasma [46]. Since total pressure increase is known to be responsible for the formation of argon plasma with higher density and therefore higher ionic current, it consequently leads to a deposition rate increase (figure 2).

Furthermore, total pressure increase is found to be responsible for an intrinsic stress increase from very compressive to very tensile values (figure 3). This transition was already evidenced in literature [47-49]. Given the fact that this transition was found to depend on tungsten film's density and microstructure [47,49], the intrinsic stress origin into sputtered tungsten films was not fully explained. It is assumed that the compressive stress is related to atomic peening of the film due to particles bombardment during sputtering deposition process and that total pressure increase is responsible for plasma particles thermalization that induces tensile stress [48,50]. Nevertheless, this compressive-tensile stress transition yields a no-stress tungsten film. Such condition of no-stress (or slightly tensile stress) is very important in order to be able to deposit tungsten films with various thicknesses without encountering non-adhesion and/or delamination phenomena. Given our sputtering conditions (bias: 0 V, power: 800 W), this no-stress film was obtained for an argon total pressure of $20 \times 10^{-3}$ millibars. The aforementioned experimental conditions were finally used for the integration of ($W/WO_3$ – Pt – Ag/AgCl) ElecCell microdevices.

Finally, the tungsten film's resistivity was found to be at least two or three times higher than the one obtained with the bulk material (around 5 μΩcm [50]). This ratio was already found in literature and is related to impurities systematically introduced in the films during sputtering process [51]. According our results, argon total pressure increase induces a resistivity increase. Nevertheless further conclusions can hardly be provided for contradictory reasons. On one side according to the grain-boundaries model [52], resistivity depends on the film's thickness and not on the deposition rate. On the other side, in disagreement with the grain-boundaries model, the use of argon-based plasma was found to be responsible for complex resistivity variations with film thickness due to huge discrepancies in terms of microstructure, morphology and porosity [46]. These variations were related to the deposition of different tungsten phases α–W and β-W according to the deposition parameters: plasma power, temperature and pressure [51,53]. However, coming back to our main interest, resistivity values obtained for the no-stress tungsten film (~ 16.5

μΩcm) were low enough to enable use of such film for the development of microelectrodes and electrochemical microcells.

### 3.2 Characterization of the integrated Ag/AgCl reference electrode

In order to validate the integrated Ag/AgCl reference electrode, its behaviour was studied for the measurement of chloride ion ($Cl^-$) concentration in liquid phase using a Metrohm Ag/AgCl glass double junction reference electrode. Typical potentiometric responses were obtained for the Nernst potential at equilibrium, yielding quasi-Nernstian sensitivities of 57 ± 2 mV/pCl on the [$10^{-5}$ M – $10^0$ M] concentration range (figure 4) [54-56]. Then, its stability was studied in 0.01M KCl solutions with different pH (pH= 2.0, 7.0 and 12.0) (figure not shown). Whatever the pH (i.e. acid, neutral or basic), after an initial decrease of around 5 mV during half an hour, the Ag/AgCl microelectrode's potential at equilibrium was found to be quite stable with a value of around 0.10 V, exhibiting a very low negative drift (around 3 mV/h) during one hour. Such result is in agreement with literature [54,56] and validates our microfabrication process based on thin, i.e. micrometric or smaller, metallic films and passivation layers.

### 3.3 pH measurement using $W/WO_3$ and $Pt/IrO_2$ microelectrodes

Measurement properties of the different pH-sensitive microelectrodes were studied in different solutions (pH = 2.0, 4.0, 5.5, 7.0, 8.5, 10.0 and 12.0) while keeping chloride ion concentration constant to avoid any interference associated to the integrated Ag/AgCl reference electrode. Nevertheless, in a first step, both $Pt/IrO_2$ and $W/WO_3$ microelectrodes were studied using a Metrohm commercial reference electrode. As expected, both microelectrodes were found to be sensitive to pH and be able to monitor pH variations from 2 to 12 (figures 5 and 6). So, $Pt/IrO_2$

microelectrodes yielded Nernstian sensitivity (around 60 mV/pH) [14-18,24-27]. It should be mentioned that literature showed supra-Nernstian pH responses for AEIROF-based microelectrodes and related them to variations in the $IrO_2$ oxidation state [12,19,20,22,23,25]. In our case, such improved sensitivity values were not obtained. Concerning tungsten oxide based microelectrodes, they exhibited linear, sub-Nernstian sensitivity (around 55 mV/pH). Such value is representative of stoichiometric tungsten oxide $WO_3$ rather than non-stoichiometric oxide [38,41,42].

Measurement stability was also examined for three different solutions (pH = 2.0, 7.0 and 12.0) during several hours. It should be mentioned that no deterioration of the $W/WO_3$ structure was noticed during these experiments. Both $Pt/IrO_2$ and $W/WO_3$ microelectrodes were characterized by a similar temporal drift around 6 mV/h, i.e. 0.1 pH/h (results not shown). Such low values should be related to the silicon-based thin-film fabrication process. According to these results, hysteresis was studied for the acid/basic/acid transition. Thus, a low value (around 5 mV) was obtained for the $Pt/IrO_2$ microelectrodes whereas a higher one (around 50 mV) was found for the $W/WO_3$ microelectrode. Such result could be related to the electrochemical stability of tungsten oxides in water-based solutions. According to the metastable E-pH diagram proposed for the $WO_3$-$H_2O$ system [38,57], the formation of tungstate ions ($WO_4^{2-}$) occurs for pH higher than 6. A careful analysis of our experimental results (figure 6) demonstrate a potential shift of 50 mV around pH = 6, correlating the high hysteresis value to electrochemical instabilities of $WO_3$ films obtained through oxygen ($O_2$) plasma oxidation. This phenomenon is quite problematic since it will be responsible for possible measurement errors at neutral pH. Nevertheless, this should be solved by improving the tungsten oxidation process [42].

Then, ($Pt/IrO_2$ – Ag/AgCl) and ($W/WO_3$ - Ag/AgCl) pH-sensitive microdevices were used for pH monitoring in an autonomous way, i.e. using the integrated Ag/AgCl reference microelectrode (rather than the Metrohm commercial reference electrode as reported previously). In both cases, pH was monitored successfully, demonstrating the integration of pH-sensitive potentiometric

microcells using iridium oxide $IrO_2$ or tungsten oxide $WO_3$ sensitive layers (figure 7). According to calibration curves (figure 8) and as previously reported, the Pt/$IrO_2$-based pH-ElecCell yielded higher sensitivity compared to the W/$WO_3$-based one, i.e. 60 versus 55 mV/pH (table 2). Concerning stability at pH 2.0, 7.0 and 12.0, a temporal drift of approximately 18 mV/hour, i.e. 0.3 pH/h, was obtained (results not shown). Compared to the previous result, the increase should be directly correlated to the use of the integrated Ag/AgCl reference microelectrode. Firstly, its own temporal drift (~ 3 mV/h, cf. §3.2) is interfering with the final pH measurement. Secondly, the electrical polarization of the whole microdevices should be responsible for leakage currents between microelectrodes due to technological defects at the wafer level. From a measurement reproducibility point of view, such high temporal drift should strongly hinder the long-term use of the examined technology. Nevertheless, it can be reduced by developing specific techniques not only on wafer-level but also regarding and (micro)system packaging techniques [58-60]. Finally, as previously reported, the W/$WO_3$-based pH-ElecCell yielded higher hysteresis compared to the Pt/$IrO_2$-based one: -25 mV versus +75 mV. Similarly, the discrepancy is clearly related to some potential variation occurring around pH 6 and previously associated to the formation of tungstic acid $H_2WO_4$ [38,57]. Finally, the hysteresis value obtained for the Pt/$IrO_2$-based pH-sensitive microdevices was not clearly understood. It should be related to the use of the integrated Ag/AgCl reference electrode and needs to be further studied.

Overall, the different results related to pH detection were summarized in table 2. Thus, it appears that the Pt/$IrO_2$-based pH-ElecCell is better compared to the W/$WO_3$-based microdevice. Nevertheless, these lower performances are fully counterbalanced by the fact that W/$WO_3$-based pH-ElecCell is mass fabricated due to tungsten layer oxidation using an oxygen $O_2$ plasma process while Pt/$IrO_2$-based microdevice is still fabricated individually through to a standard anodic electrodeposition process.

## 4. Conclusion

A silicon-based technological platform dedicated to (Pt – Pt – Ag/AgCl) electrochemical microcells (ElecCell) was used to fabricate ($Pt/IrO_2$ – Ag/AgCl) and ($W/WO_3$ – Ag/AgCl) potentiometric microdevices. Specific attention was brought on the mass fabrication of the $W/WO_3$ microelectrode. As a matter of fact, a no-stress thin tungsten film was deposited by sputtering in order to avoid any non-adhesion and/or delamination problems, and was then oxidized through an oxygen ($O_2$) plasma process to mass fabricate the tungsten oxide thin layer. Compared to the $Pt/IrO_2$-based one, the $W/WO_3$-based microdevices showed lower performances concerning pH measurement. Nevertheless, since quasi-Nernstian sensitivity (around 55 mV/pH) as well as acceptable stability (around 18 mV/h) and hysteresis (around 50 mV) were evidenced on the [2-12] pH range, ($W/WO_3$ – Ag/AgCl) pH-sensitive microdevices were successfully developed for pH monitoring in liquid phase. As a result, tungsten oxide $WO_3$ was finally found to be a good candidate for the mass fabrication of pH microsensors using silicon-based technologies.

From our results, two drawbacks still need to be solved. First, even if fabrication reproducibility is ensured by the use of a well-defined, silicon-based process, measurement reproducibility is still hindered by relatively high temporal drifts: values around 6 or 18 millivolts per hour, i.e. 0.1 or 0.3 pH per hour, were evidenced according to the use of the integrated Ag/AgCl reference microelectrode. This drawback appears to be not related to working electrode materials, i.e. $Pt/IrO_2$ or $W/WO_3$, but to the technological compatibility between potentiometric devices and liquid phase analysis. Secondly, the $WO_3/H_2WO_4$ transition at pH 6 was found to be responsible for measurement instabilities and finally high hysteresis (around 50 mV). Both drawbacks will be solved through technological process improvements associated with the tungsten plasma oxidation process under oxygen ($O_2$) as well as wafer-level and/or (micro)system packaging procedures.

**Acknowledgements**

Technological realizations were partly supported by the French RENATECH network.

**References**

[1] W. Vonau and U. Guth: "pH monitoring: a review", Journal of Solid State Electrochemistry, 10 (2006) 746-752

[2] http://www.biomerieux-diagnostics.com/servlet/srt/bio/clinical-diagnostics/dynPage?doc=CNL_PRD_CPL_G_PRD_CLN_11

[3] http://www.sentron.nl/ph-meters/ph-meter-line/

[4] P. Bergveld: "Thirty years of ISFETOLOGY: what happened in the past 30 years and what may happen in the next 30 years", Sensors and Actuators, B88 (2003), 1-20

[5] A. Yamada, S. Mohri, M. Nakamura and K. Naruse: "A fully automated pH measurement system for 96-well microplates using a semiconductor-based pH sensor", Sensors and Actuators, B143 (2010) 464-469

[6] M.L. Pourciel Gouzy, W. Sant, I. Humenyuk, L. Malaquin, X. Dollat and P. Temple-Boyer: "Development of pH-ISFET sensors for the detection of bacterial activity", Sensors and Actuators, B103 (2004) 247-251

[7] E. Thedinga, A. Kob, H. Holst, A. Keuer, S. Drechsler, R. Niendorf, W. Bauman, I. Freund, M. Lehman and R. Ehret: "On-line monitoring of cell metabolism for studying pharmacodynamic effects", Toxicology and Applied Pharmacology, 220 (2007) 33-44

[8] W. Sant, P. Temple-Boyer, E. Chanié, J. Launay and A. Martinez: "On-line monitoring of urea using enzymatic field effect transistors", Sensors and Actuators, B160 (2011) 59-64

[9] J. Rothberg, W. Hinz, T. Rearick, J. Schultz, W. Mileski, M. Davey, J. Leamon, K. Johnson, M. Milgrew, M. Edwards, J. Hoon, J. Simons, D. Marran, J. Myers, J. Davidson, A. Branting, J. Nobile, B. Puc, D. Light, T. Clark, M. Huber, J. Branciforte, I. Stoner, S. Cawley, M. Lyons, Y. Fu, N. Homer, M. Sedova, X. Miao, B. Reed, J. Sabina, E. Feierstein, M. Schorn, M. Alanjary, E. Dimalanta, D. Dressman, R. Kasinskas, T. Sokolsky, J. Fidanza, E. Namsaraev, K. McKernan, A. Williams, T. Roth and J. Bustillo: "An integrated semiconductor device enabling non-optical genome sequencing", Nature, 475 (2011) 348-352

[10] A. Fog and R.P. Buck: "Electronic semiconducting oxides as pH sensors", Sensors and Actuators, 5 (1984) 137-146

[11] K. Yamanaka: "Anodically electrodeposited iridium oxide films (AEIROF) from alkaline solutions for electrochromic display devices", Japanese Journal of Applied Physics, 28 (1989) 632-637

[12] W. Olthuis, M.A.M. Robben, P. Bergveld, M. Bos and W.E. Van der Linden: "pH sensor properties of electrochemically grown iridium oxides", Sensors and Actuators, 2 (1990) 247-256

[13] M.A. Petit and V. Plichon: "Anodic electrodeposition of iridium oxide films", Journal of Electroanalytical Chemistry, 444 (1998) 247-252

[14] S.A.M. Marzouk, S. Ufer and R.P. Buck: "Electrodeposited iridium oxide pH electrodes for measurement of extracellular myocardial acidosis during acute aschemia", Analytical Chemistry, 70 (1998) 5054-5061

[15] A.N. Bezbaruah and T.C. Zhang: "Fabrication of anodically electrodeposited iridium oxide film pH microelectrodes for microenvironmental studies", Analytical Chemistry, 74 (2002) 5726-5733

[16] M. Wang, S. Yao and M. Madou: "A long-term stable iridium oxide pH electrode", Sensors and Actuators, B81 (2002) 313-315

[17] T.-Y. Kim and S. Yang: "Fabrication method and characterization of electrodeposited and heat-treated iridium oxide films for pH sensing", Sensors and Actuators, B196 (2014) 31-38

[18] A. Tsopela, A. Lale, E. Vanhove, O. Reynes, I. Séguy, P.J. Juneau, R. Izquierdo, P. Temple-Boyer and J. Launay: "Integrated electrochemical biosensor based on algal metabolism for water toxicity analysis", Biosensors and Bioelectronics, 61 (2014) 290-297

[19] E. El-Deen, M. El-Giar and D.O. Wipf: "Microparticle-based iridium oxide ultra-microelectrodes for pH sensing and imaging", Journal of Electroanalytical Chemistry, 609 (2007) 147-157

[20] E. Prats-Alfonso, L. Abad, N. Casan-Pastor, J. Gonzalo-Ruiz and E. Baldrich: "Iridium oxide pH sensor for biomedical applications, case urea-urease in real urine samples", Biosensors and Bioelectronics, 39 (2013) 163-169

[21] S.C. Mailley, M. Hyland, P. Mailley, J.M. MacLaughlin and E.T. Adams: "Electrochemical and structural characterizations of electrodeposited iridium-oxide thin-film electrodes applied to neurostimulating electrical signals", Materials Science and Engineering, 21 (2002) 167-175

[22] I.A. Ges, B.L. Ivanov, D.K. Schaffer, E.A. Lima, A.E. Werdich and F.J. Baudenbacher: "Thin-film $IrO_x$ pH microelectrodes for fluidic-based microsystems", Biosensors and Bioelectronics, 21 (2005) 248-256

[23] I.A. Ges, B.L. Ivanov, A.E. Werdich and F.J. Baudenbacher: "Differential pH measurements of metabolic cellular activity in nL cultures volumes using microfabricated iridium oxide electrodes", Biosensors and Bioelectronics, 22 (2007) 1303-1310

[24] C.-C. Wu, W.-C. Lin and S.-Y. Fu: "The open container-used microfluidic chip using $IrO_x$ ultramicroelectrodes for the in situ measurement of extracellular acidification", Biosensors and Bioelectronics, 26 (2011) 4194-4197

[25] M.F. Smiechowski and V.F. Lvovich: "Iridium oxide sensors for acidity and basicity detection in industrial lubricants", Sensors and Actuators, B96 (2003) 261-267

[26] T. Katsube, I. Lauks and J.N. Zemel: "pH-sensitive sputtered iridium oxide films", Sensors and Actuators, 2 (1982) 399-410

[27] K.G. Kreider, M.J. Tarlov and J.P. Cline: "Sputtered thin-film pH electrodes of platinum, palladium, ruthenium and iridium oxides", Sensors and Actuators, B28 (1995) 167-172

[28] K. Nishio, Y. Watanabe and T. Tsuchiya: "Preparation and properties of electrochromic iridium oxide thin film by sol-gel process", Thin Solid Films, 350 (1999) 96-100

[29] W.-D. Huang, H. Cao, S. Deb, M. Chiao and J.C. Chiao: "A flexible pH sensor based on the iridium oxide sensing film", Sensors and Actuators, B169 (2011) 1-11

[30] K.Y. Ahn: "A comparison of tungsten film deposition techniques for very large scale integration technology", Thin Solid Films, 153 (1987) 469-478

[31] S. Schmidbauer, J. Hahn, A. Buerke, F. Jakubowski, O. Storbeck, Y.-W. Ting, T. Schuster and J. Faul: "Interface optimization for polysilicon/tungsten gates", Microelectronic Engineering, 85 (2008) 2037-2041

[32] J.L. He and M.C. Chiu: "Effect of oxygen on the electrochromism of RF reactive magnetron sputter deposited tungsten oxide", Surface and Coatings Technology, 127 (2000) 43-51

[33] C. Brigouleix, P. Topart, E. Bruneton, F. Sabary, G. Nouhaut and G. Campet: "Roll-to-roll pulsed DC magnetron sputtering of $WO_3$ for electrochromic windows", Electrochimica Acta, 46 (2001) 1931-1936

[34] B. Marsen, E.L. Miller, D. Paluselli and R.E. Rocheleau: "Progress in sputtered tungsten trioxide for photoelectrode applications", International Journal of Hydrogen Energy, 32 (2007) 3110-3115

[35] A. Subrahmanyam and K. Karruppasamy: "Optical and electrochromic properties of oxygen sputtered tungsten oxide ($WO_3$) films", Solar Energy Materials & Solar Cells, 91 (2007) 266-274

[36] M.J. Natan, T.E. Mallouk and M.S. Wrighton: "pH-sensitive $WO_3$-based microelectrochemical transistors", Journal of Physical Chemistry, 91 (1987) 648-654

[37] L.T. Dimitrakopoulos, T. Dimitrakopoulos, P.W. Alexander, D. Logic and D.B. Hibbert: "A tungsten oxide coated wire electrode used as a pH sensor in flow injection potentiometry", Analytical Communications, 35 (1998) 395-398

[38] M. Anik: "Anodic behavior of tungsten in $H_3PO_4$-$K_2SO_4$-$H_2SO_4$/KOH solutions", Turkish Journal of Chemistry, 26 (2002) 915-924

[39] K. Yamamoto, G. Shi, T. Zhou, F. Xu, M. Zhu, M. Liu, T. Kato, J.-Y. Jin and L. Jin: "Solid-state pH ultramicrosensor based on tungstic oxide film fabricated on a tungsten nanoelectrode and its application on the study of endothelial cells", Analytica Chimica Acta, 480 (2003) 109-117

[40] A. Ruffien-Ciszak, J. Baur, P. Gros, E. Questel and M. Comtat: "Electrochemical microsensors for cutaneous surface analysis: application to the detection of pH and the antioxidant properties of *stratum corneum*", ITBM-RBM, 29 (2008) 162-170

[41] I.A. Pasti, T. Lazarevic Pasti and S.V. Mentus: "Switching between voltammetry and potentiometry in order to determine $H^+$ or $OH^-$ ion concentration over the entire pH scale by means of tungsten disk electrode", Journal of Electroanalytical Chemistry, 665 (2012) 83-89

[42] Y. Wen, and X. Wang: "Characterization and application of a metallic tungsten electrode for potentiometric pH measurements", Journal of Electroanalytical Chemistry, 714-715 (2014) 45-50

[43] G.G. Stoney: "The tension of metallic films deposited by electrolysis", Proceedings of the Royal Society of London, 9 (1909) 172-175

[44] C. Christophe, F. Sekli Belaidi, J. Launay, P. Gros, E. Questel and P. Temple-Boyer: "Elaboration of integrated microelectrodes for the detection of antioxidant species", Sensors and Actuators, B177 (2013) 350-356

[45] E. Vanhove, A. Tsopela, L. Bouscayrol, A. Desmoulin, J. Launay and P. Temple-Boyer: "Final capping passivation layers for long-life microsensors in real fluids", Sensors and Actuators, B178 (2013) 350-358

[46] F. Meyer, C. Schwebel, C. Pellet and G. Gautherin: "Characterization of ion-beam-sputtered tunsten films on silicon", Applied Surface Science, 36 (1989) 231-239

[47] M.C. Hugon, F. Varnière, B. Agius, M. Froment, C. Arena and J. Bessot: "Stresses, microstructure and resistivity of thin tunsten films deposited by RF magnetron sputtering", Applied Surface Science, 38 (1989) 269-285

[48] M. Mamor, E. Dufour Gergam, L. Finkman, G. Tremblay, F. Meyer and K. Bouziane: "W/Si Schottky diodes: effect of sputtering deposition conditions on the barrier height", Applied Surface Science, 91 (1995) 342-346

[49] G. Zazarra and I.E. Reimanis: "Residual stresses in the failure of W-Pt-Ag metallizations on oxidized Si", Surface and Coatings Technology, 111 (1999) 92-96

[50] J.A. Thornton and D.W. Hoffman: "Stress-related effects in thin films", Thin Solid Films, 171 (1989) 5-31

[51] S.M. Rossnagel, I.C. Noyan and C. Cabral: "Phase transformation of thin sputter-deposited tungsten films at room temperature", Journal of Vacuum Science and Technology, B20 (2002) 2047-2051

[52] A.F. Mayadas and M. Schatzkes: "Electrical resistivity model for polycrystalline films: the case of arbitrary reflection at external surfaces", Physical Review, B1 (1970) 1382-1389

[53] P. Petroff, T.T. sheng, A.K. Sinha, G.A. Rozgonyi and F.B. Alexander, I.C. Noyan and C. Cabral: "Microstructure, growth, resistivity and stresses in thin tungsten films deposited by RF sputtering", Journal of Applied Physics, 44 (1973) 2545-2554

[54] L. Tymecki: "Screen-printed reference electrodes for potentiometric measurements", Analytica Chimica Acta, 526 (2004) 3-11

[55] M.W. Shinwari: "Microfabricated reference electrodes and their biosensing applications", Sensors, 10 (2010) 1679-1715

[56] A. Cazalé, W. Sant, J. Launay, F. Ginot and P. Temple-Boyer: "Study of field effect transistors for the sodium detection using fluorosiloxane-based sensitive layers", Sensors and Actuators, B177 (2013) 515-521

[57] M. Anik and K. Osseo-Assare: "Effect on pH on the anodic behavior of tungsten", Journal of the Electrochemical Society, 149 (2002) B224-B233

[58] M.L. Pourciel-Gouzy, S. Assié-Souleille, L. Mazenq, J. Launay and P. Temple-Boyer: "pH-ChemFET-based analysis devices for the bacterial activity monitoring", Sensors and Actuators, B134 (2008) 339-344

[59] P. Temple-Boyer, J. Launay, I. Humenyuk, T. Do Conto, A. Martinez, C. Bériet and A. Grisel: "Study of front-side connected chemical field effect transistor for water analysis", Microelectronics Reliability, 44 (2004) 443-447

[60] I. Humenyuk, P. Temple-Boyer and G. Sarrabayrouse: "The effect of sterilization on the pH-ChemFET behaviour", Sensors and Actuators, A147 (2008) 165-168

**Biographies**

Ahmet Lale was born in Lyon, France, on July 13, 1985. He received his Master's degree in micro-electronics/micro-systems from the Paul Sabatier University of Toulouse (France) in 2012. He joined the "Laboratoire d'Analyse et d'Architecture des Systèmes" (LAAS) of the "Centre National de la Recherche Scientifique" (CNRS) of Toulouse in 2012 as a PhD student. He works on the development of electrochemical micro/nanosensors for chemical and biochemical detection.

A. Tsopela was born in Athens, Greece in 1988. She received the master degree in Chemical Engineering from the National Technical University of Athens (NTUA - Greece), in 2011. She joined the "Laboratoire d'Architecture et d'Analyse des Systèmes" of the "Centre National de la Recherche Scientifique" (LAAS-CNRS), in 2011 as PhD Student. She is carrying out her experimental research in the development of microsensors with environmental applications.

Aurélie Civélas was born in Aix-en-Provence, France, on January 12 1989. She joined the "Laboratoire d'Analyse et d'Architecture des Systèmes" (LAAS) of the "Centre National de la Recherche Scientifique" (CNRS) of Toulouse in 2012 for a one year training course. She worked on the development of electrochemical microsensors for chemical and biochemical detection. She received the degree in electronic Engineering from the in "Chimie - Physique – Electronique" school (Lyon – France) in 2014.

L. Salvagnac was born on May 9, 1970 in Toulouse. He received his Master's Degree in nuclear maintenance from the University of Toulouse (France), in 1995. In 1997, he joined the "Laboratoire d'Architecture et d'Analyse des Systèmes" of the "Centre National de la Recherche Scientifique" (LAAS-CNRS) in the "Techniques and Equipments Applied to Microelectronics" (TEAM) service as an engineer. He is working on the development of physical vapour deposition (PVD) processes technologies for the manufacture of integrated microdevices.

Jérôme Launay was born on March 11, 1975. He received the degree in electronic engineering from the Institut National des Sciences Appliquées de Toulouse" (France) in 1998. He joined the "Laboratoire d'Architecture et d'Analyse des Systèmes" from the French "Centre National de la Recherche Scientifique" (LAAS-CNRS) in 1998 and received the PhD degree from the "Institut National des Sciences Appliquées de Toulouse" (France) in 2001. In 2002, he became lecturer at the

University of Toulouse (France). His research activities include the development of electrochemical microsensors for the detection in liquid phase.

Pierre Temple-Boyer was born on October 25, 1966. He received his Engineer's Degree in electronic engineering from the "Ecole Supérieure d'Electricité" (Paris – France) in 1990 and his Master's Degree in microelectronics from the University of Toulouse (France) in 1992. He joined the "Laboratoire d'Architecture et d'Analyse des Systèmes" (LAAS) from the French "Centre National de la Recherche Scientifique" (CNRS) in 1992 and received the PhD degree from the "Institut National des Sciences Appliquées de Toulouse" (France) in 1995. Since then, as a CNRS researcher, he has worked at LAAS on the development of physical and chemical microsensors.

## TABLE & FIGURE CAPTIONS

Table 1: characteristics of tungsten thin films deposited by sputtering (bias: 0 V, power: 800 W) as a function of argon total pressure (deviations were estimated through at least five different measurements on the wafer)

Table 2: Comparison of pH detection properties of $Pt/IrO_2$–based and $W/WO_3$-based potentiometric microdevices (deviations were estimated by characterizing three $Pt/IrO_2$ and six $W/WO_3$ microelectrodes)

Figure 1: a) optical and (inset) scanning electron microscopy (SEM) of ($W/WO_3$ – Pt – Ag/AgCl) electrochemical microcell chips and b) SEM and (inset) optical micrographs of ($Pt/IrO_2$ – Pt – Ag/AgCl) electrochemical microcell chips

Figure 2: variations of the sputtered tungsten deposition rate as a function of argon total pressure (linear fit is given by the dotted line, error bars represent standard deviation across at least five measurements)

Figure 3: variations of the sputtered tungsten film intrinsic stress as a function of argon total pressure (linear fit is given by dotted line, error bars represent standard deviation across at least five measurements)

Figure 4: pCl calibration curve of the integrated Ag/AgCl reference electrode (linear fit is given by dotted line, error bars represent standard deviation across at least nine measurements)

Figure 5: pH analytical responses of a) $W/WO_3$ and b) $Ti/Pt/IrO_2$ microelectrodes using a Metrohm commercial reference electrode

Figure 6: pH calibration curves of $W/WO_3$ and $Pt/IrO_2$ microelectrodes using a Metrohm commercial reference electrode (linear fits are given by dotted lines, error bars represent standard deviation across at least nine measurements)

Figure 7: pH analytical responses of a) ($W/WO_3$ –Ag/AgCl) and b) ($Pt/IrO_2$ – Ag/AgCl) potentiometric microdevices

Figure 8: pH calibration curves of ($W/WO_3$ – Ag/AgCl) and ($Pt/IrO_2$ – Ag/AgCl) potentiometric microdevices (linear fits are given by dotted lines error bars represent standard deviation across at least nine measurements)

| total pressure (millibar) | deposition rate (nm/min) | residual stress (GPa) | resistivity (μΩcm) |
|---|---|---|---|
| $1 \times 10^{-3}$ | 77 ± 4 | - 2.6 ± 0.13 | 13.7 ± 0.7 |
| $5 \times 10^{-3}$ | 83 ± 4 | - 2.3 ± 0.12 | 14.0 ± 0.5 |
| $10 \times 10^{-3}$ | 87 ± 4 | - 1.9 ± 0.1 | 13.5 ± 1.0 |
| $20 \times 10^{-3}$ | 96 ± 3 | 0.1 ± 0.1 | 16.5 ± 0.5 |
| $22 \times 10^{-3}$ | 100 ± 3 | 0.7 ± 0.1 | 16.5 ± 0.5 |
| $30 \times 10^{-3}$ | 133 ± 3 | 1.3 ± 0.1 | 33 ± 1 |

Table 1: characteristics of tungsten thin films deposited by sputtering

(bias: 0 V, power: 800 W) as a function of argon total pressure

(deviations were estimated through at least five different measurements on the wafer)

| | sensitivity (mV/pH) | temporal drift (mV/h) | hysteresis (mV) |
|---|---|---|---|
| $Pt/IrO_2$ microelectrode vs reference electrode | 60 ± 1 | 6 ± 1.5 | +5 ± 0.5 |
| $W/WO_3$ microelectrode vs reference electrode | 55 ± 1 | 6 ± 1.5 | -50 ± 2 |
| ($Pt/IrO_2$ - Pt - Ag/AgCl) ElecCell | 60 ± 1 | 18 ± 3 | +25 ± 1 |
| ($W/WO_3$ - Pt - Ag/AgCl) ElecCell | 55 ± 1 | 18 ± 3 | -75 ± 5 |

Table 2: Comparison of pH detection properties

of $Pt/IrO_2$–based and $W/WO_3$-based potentiometric microdevices

(deviations were estimated by characterizing three $Pt/IrO_2$ and six $W/WO_3$ microelectrodes)

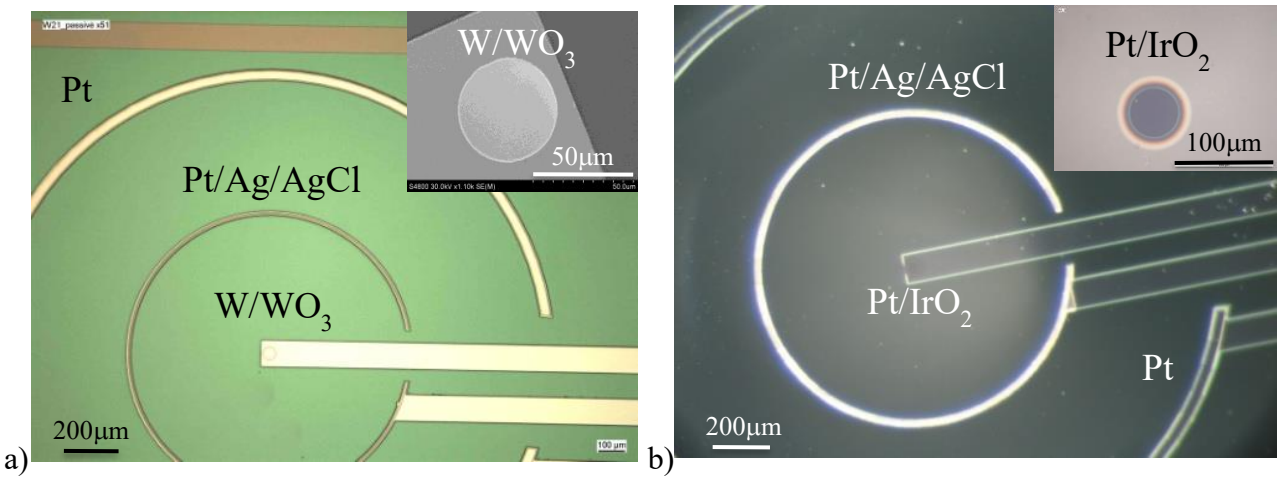


Figure 1: a) optical and (inset) scanning electron microscopy (SEM) of ($W/WO_3$ – Pt – Ag/AgCl) electrochemical microcell chips and b) SEM and (inset) optical micrographs of ($Pt/IrO_2$ – Pt – Ag/AgCl) electrochemical microcell chips

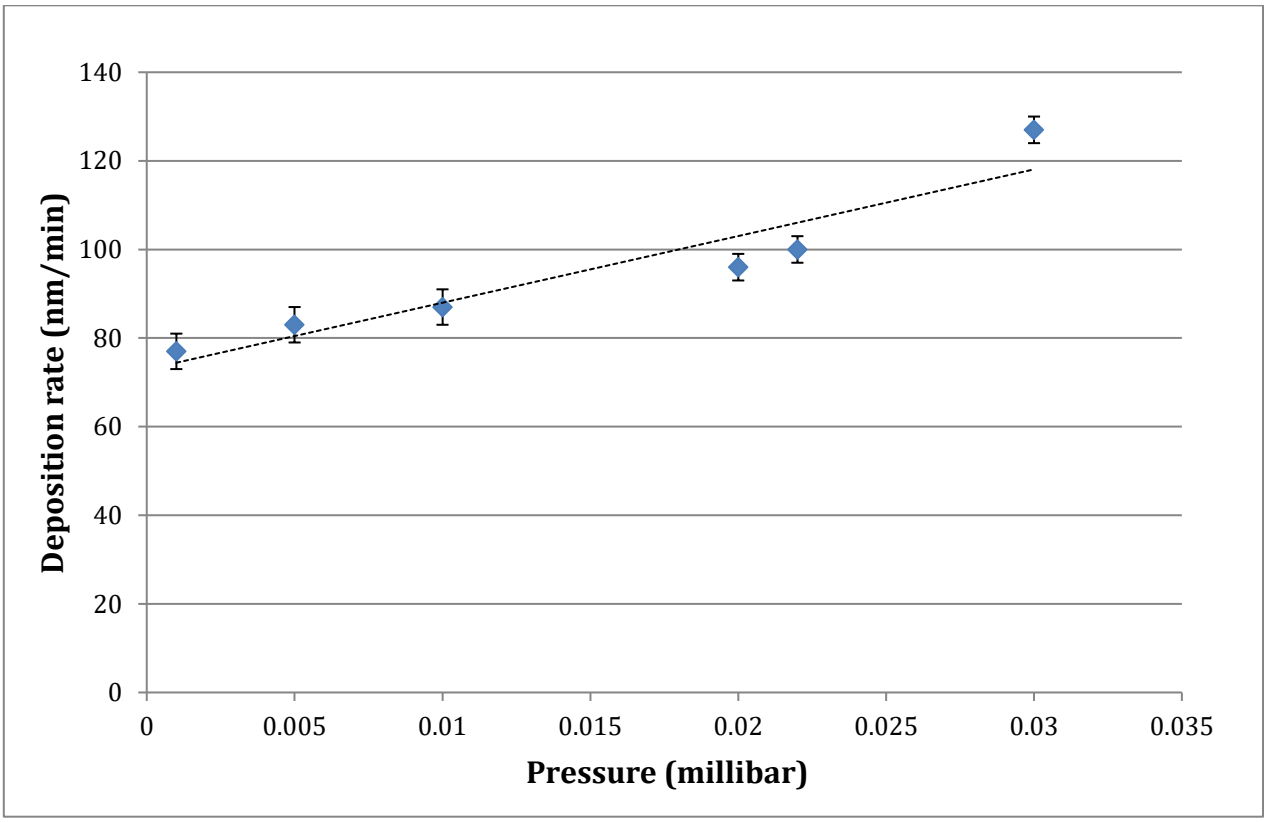


Figure 2: variations of the sputtered tungsten deposition rate as a function of argon total pressure (linear fit is given by the dotted line, error bars represent standard deviation across at least five measurements)

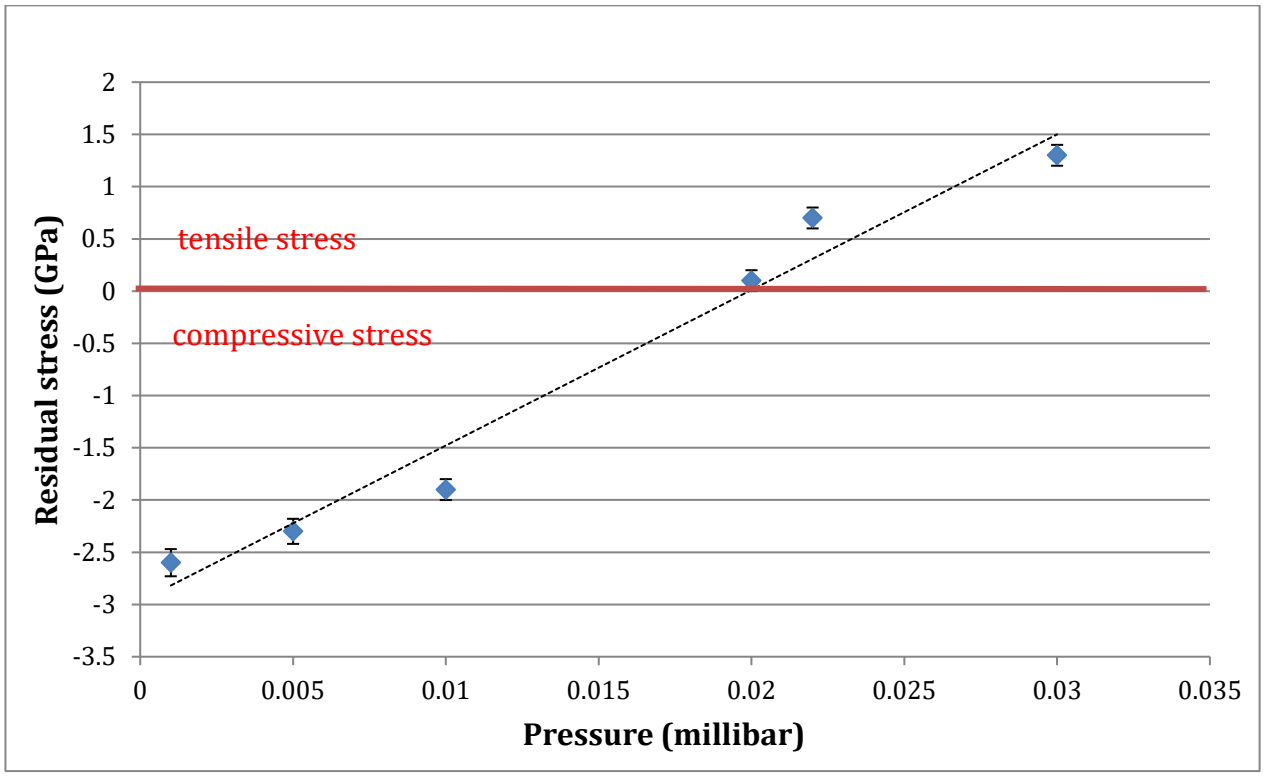


Figure 3: variations of the sputtered tungsten film intrinsic stress as a function of argon total pressure (linear fit is given by dotted line, error bars represent standard deviation across at least five measurements)

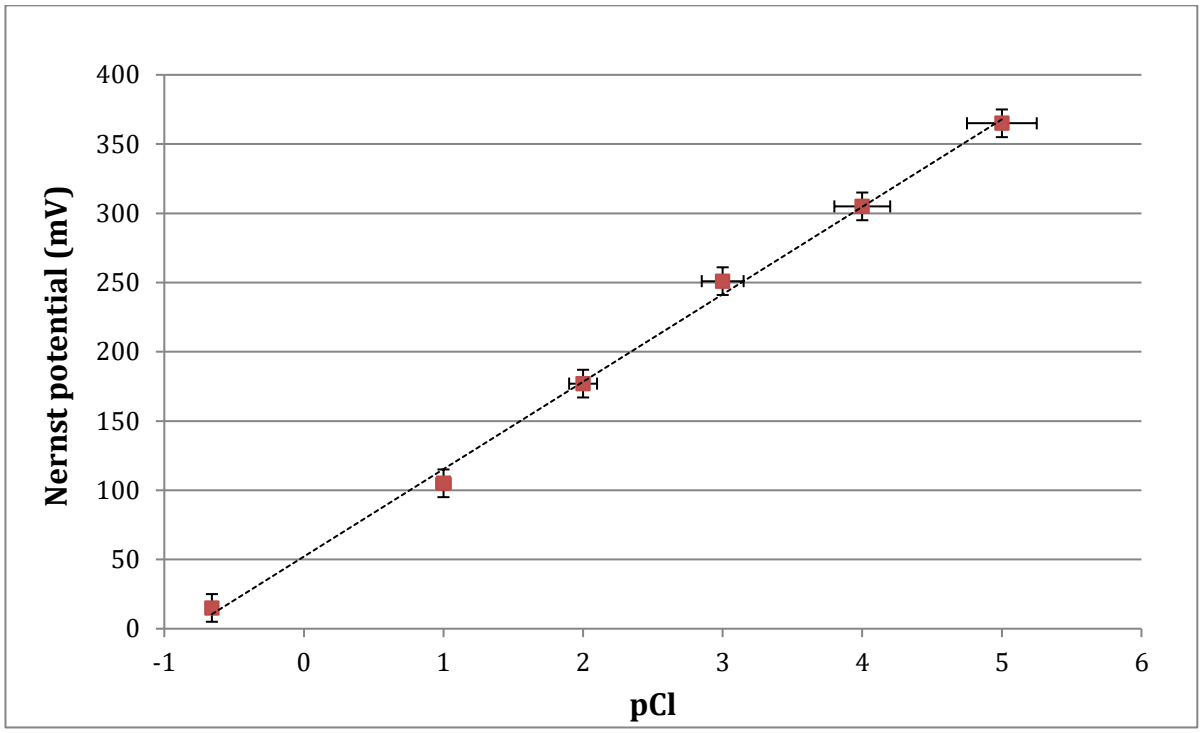


Figure 4: pCl calibration curve of the integrated Ag/AgCl reference electrode (linear fit is given by dotted line, error bars represent standard deviation across at least nine measurements)

a) 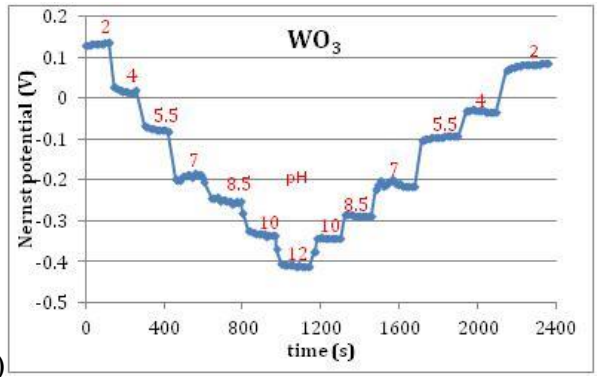

b) 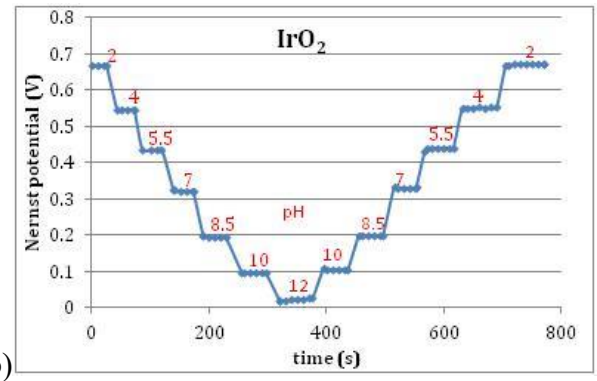


Figure 5: pH analytical responses of a) W/$WO_3$ and b) Ti/Pt/$IrO_2$ microelectrodes using a Metrohm commercial reference electrode

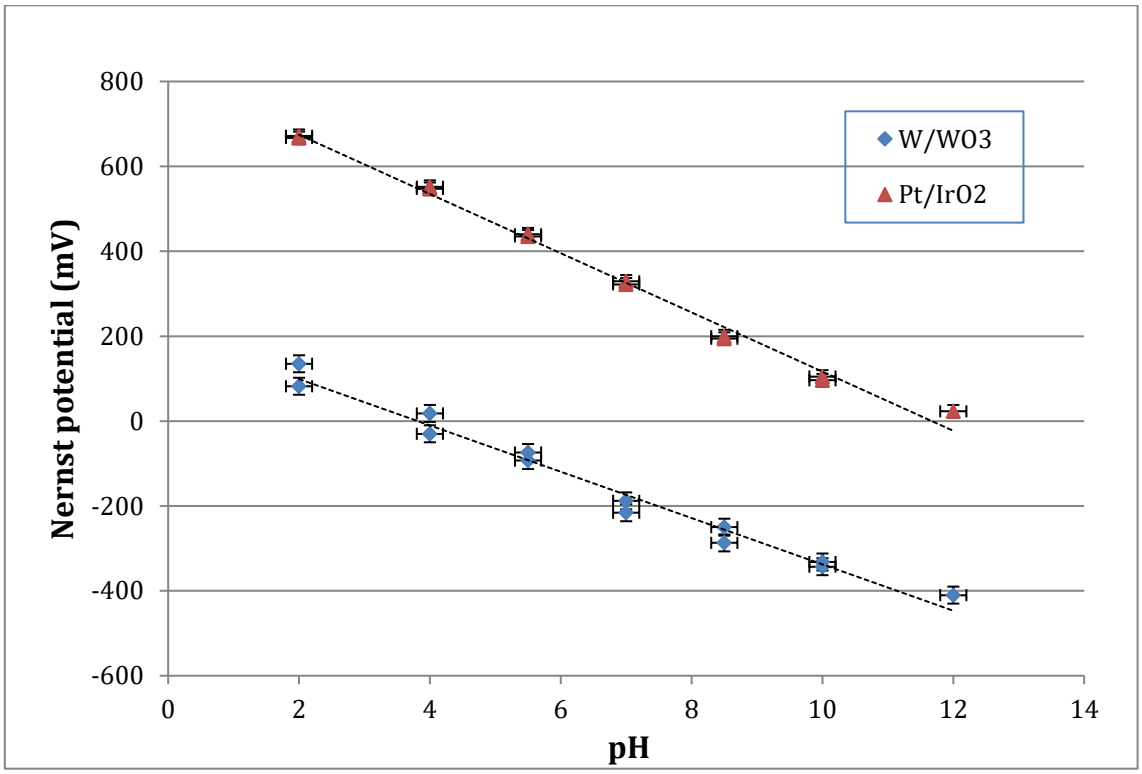


Figure 6: pH calibration curves of $W/WO_3$ and $Pt/IrO_2$ microelectrodes using a Metrohm commercial reference electrode (linear fits are given by dotted lines, error bars represent standard deviation across at least nine measurements)

a) 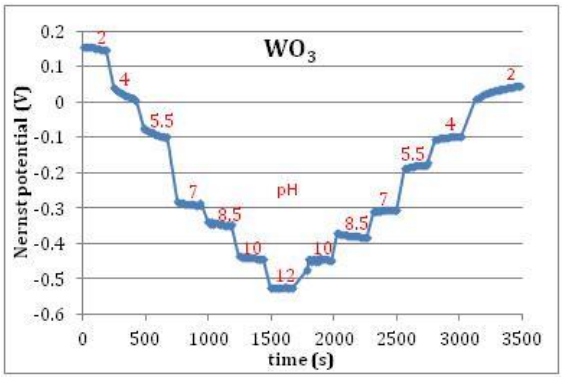


b) 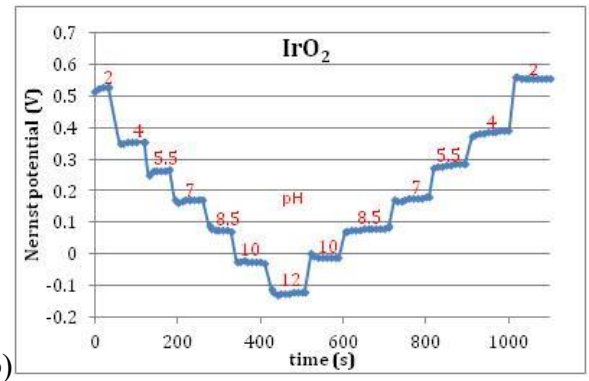


Figure 7: pH analytical responses of a) ($W/WO_3$ –Ag/AgCl) and b) ($Pt/IrO_2$ – Ag/AgCl) potentiometric microdevices

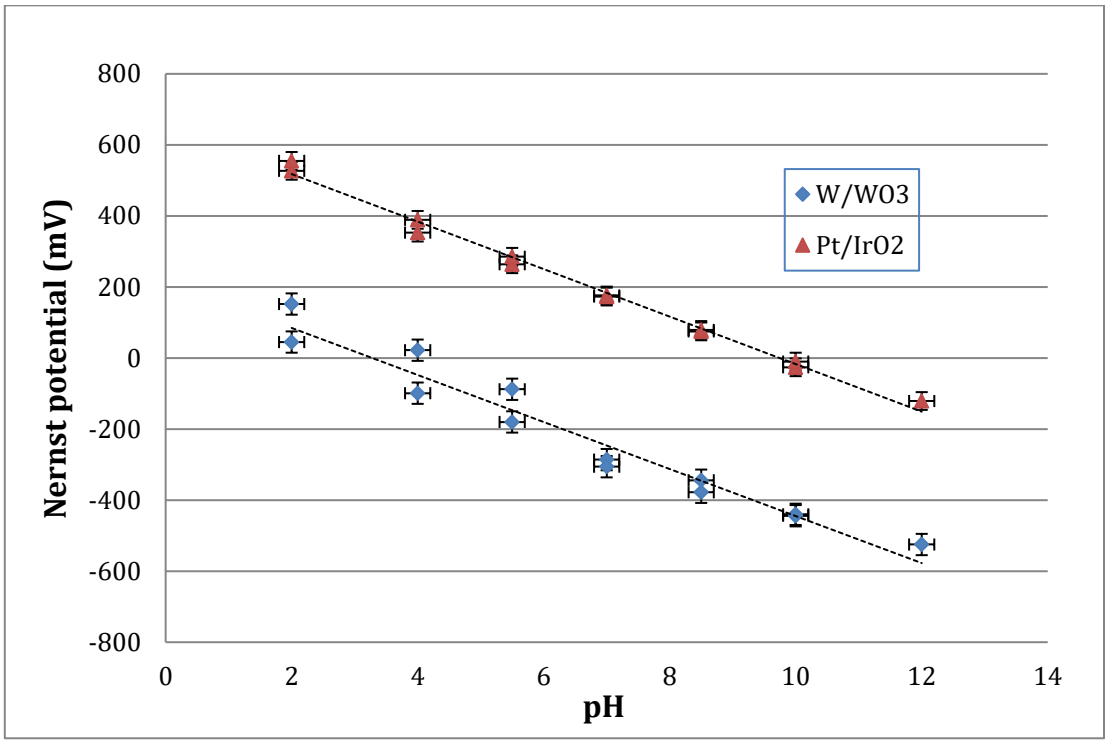


Figure 8: pH calibration curves of ($W/WO_3$ – Ag/AgCl) and ($Pt/IrO_2$ – Ag/AgCl) potentiometric microdevices (linear fits are given by dotted lines error bars represent standard deviation across at least nine measurements)